Journal of Applied Physics

RESEARCH ARTICLE | APRIL 04 2025

Ambient-pressure superconductivity above 22 K in hole-doped YB_2

Xuejie Li; Wenbo Zhao ; Yuzhou Hao; Xiaoying Wang; Zhibin Gao ; Xiangdong Ding

J. Appl. Phys. 137, 133906 (2025)
https://doi.org/10.1063/5.0256399

AIP Publishing

Journal of Applied Physics ARTICLE pubs.aip.org/aip/jap

Ambient-pressure superconductivity above 22 K in hole-doped YB_2

Cite as: J. Appl. Phys. **137**, 133906 (2025); doi: 10.1063/5.0256399
Submitted: 4 January 2025 · Accepted: 18 March 2025 ·
Published Online: 4 April 2025

View Online Export Citation CrossMark

Xuejie Li,[1] Wenbo Zhao,[2] Yuzhou Hao,[1] Xiaoying Wang,[1] Zhibin Gao,[1,a)] and Xiangdong Ding[1]

AFFILIATIONS

[1]State Key Laboratory for Mechanical Behavior of Materials, School of Materials Science and Engineering, Xi'an Jiaotong University, Xi'an 710049, China
[2]Key Laboratory of Material Simulation Methods and Software of Ministry of Education, College of Physics, Jilin University, Changchun 130012, China

[a)]**Author to whom correspondence should be addressed:** zhibin.gao@xjtu.edu.cn

ABSTRACT

Recent studies of hydrogen-dominant (superhydride) materials, such as LaH_{10}, have led to putative discoveries of near-room temperature superconductivity at high pressures, with a superconducting transition temperature (T_c) of 250 K observed at 170 GPa. While these findings are promising, achieving such high superconductivity requires challenging experimental conditions typically exceeding 100 GPa. In this study, we utilize first-principles calculations and Migdal–Eliashberg theory to examine the superconducting properties of the stable boron-based compound YB_2 at atmospheric pressure, where yttrium and boron atoms form a layered structure. Our results indicate that YB_2 exhibits a T_c of 2.14 K at 0 GPa. We find that doping with additional electrons (0–0.3) leads to a monotonic decrease in T_c. Conversely, introducing holes significantly enhances T_c, raising it to 22.83 K. Although our findings do not surpass the superconducting temperature of the well-known MgB_2, our doping strategy highlights a method for tuning electron–phonon coupling strength in metal borides. This insight could be valuable for future experimental applications. Overall, this study not only deepens our understanding of YB_2 superconducting properties but also contributes to the ongoing search for high-temperature superconductors.

I. INTRODUCTION

Superconductivity is the complete absence of electrical resistance and is observed in many materials when they are cooled below their superconducting transition temperature (T_c). In the Bardeen–Cooper–Schrieffer (BCS) theory of ("conventional") superconductivity, this occurs when electrons overcome their mutual electrical repulsion and form "Cooper pairs" that then travel unheeded through the material as a supercurrent. Low-temperature[1–3] and high-temperature superconductors are the two categories of superconducting materials. Although the most common among high-temperature superconductors, such as LaH_{10}, are currently hydrogen-based compounds,[4–6] their use is severely limited by the fact that they require extremely high pressure to achieve superconductivity.

The discovery of magnesium diboride, with a superconducting transition temperature of 39 K at ambient pressure,[7] reignited interest in metal boride superconductors with similar structures. However, the T_c of most B-related AlB_2-type structures remains below 10 K at 0 GPa, such as NbB_2 (0.62 K),[8] ScB_2 (1.5 K),[9] and $MoB_{2.5}$(8.1 K).[10] Elemental doping, such as in $Nb_{0.95}Y_{0.05}B_{2.5}$ (9.3 K) and $Mo_{0.85}Zr_{0.15}B_{2.5}$ (11.2 K),[10] is commonly employed to enhance T_c, though the impact is often limited.

Another approach involves pressure, which can raise T_c, as seen in α-MoB_2, which achieves a T_c of 37 K at 90 GPa.[11] However, this method presents challenges in practical applications. Additionally, magnesium diboride analogs with even higher transition temperatures have been identified, with bulk CaB_2 being a notable example, having an estimated T_c of around 47 K at 0 GPa,[12] though it has yet to be synthesized.

Although the T_c of most B-series compounds has been either calculated or experimentally verified, YB_2 has received relatively little attention. As a result, there is a growing belief that this compound lacks superconductivity. Contributing factors may include

low electron concentration,[10] phonon properties near the Fermi surface and Γ point due to a minor hole concentration,[13] and high ionicity in Y–B bonds.[14] However, it is noteworthy that similar B-based binary borides, such as ScB_2, have been studied within group III_B metal diborides for their superconducting properties,[9] suggesting that YB_2 has the potential to develop superconducting behavior.

According to the BCS theory, the high superconducting T_c of MgB_2 primarily arises from its high Debye temperature and strong electron–phonon coupling (EPC). Studies on the electronic structure of MgB_2 and related binary borides suggest that the metallic B layers play a crucial role in its superconductivity, particularly due to the presence of $p_{x,y}$-band holes at the Γ point. Consequently, when investigating the superconducting properties of MgB_2-type metal boride superconductors, it is essential to consider the effects of adding holes and electrons on the superconducting gaps.[15–17]

In this work, we investigate the effects of varying effective Coulomb pseudopotential parameters (μ^*), as well as the addition of holes and electrons, on superconducting gaps and T_c of YB_2 in detail. Two different software programs are used for this analysis: one based on the isotropic Migdal–Eliashberg equations[18,19] and the other on the McMillan–Allen–Dynes formula.[20] Notably, the T_c of YB_2 without any modifications is approximately 2.14 K when μ^* is set to 0.1 at 0 GPa. However, with increasing hole concentrations from 0 to 0.8, the T_c of YB_2 rises gradually at 0.7 to 22.83 K at 0 GPa, after which it falls sharply. In contrast, the addition of electrons leads to a consistent decrease in T_c. This not only shows that YB_2 is a superconductor and that its T_c can be greatly increased by adding a specific concentration of holes, but it also offers fresh insights into the research of B-system compounds, a class of superconductors that operate at atmospheric pressure.

II. COMPUTATIONAL METHODS

To investigate the structural and electronic properties of YB_2 at different hole and electron concentrations, we employed the Vienna *Ab initio* Simulation Package (VASP)[21,22] using the Perdew–Burke–Ernzerhof (PBE)[23] Generalized Gradient Approximation (GGA)[24,25] for the DFT calculations. The bare ion Coulomb potential was treated in the projector augmented wave (PAW)[21,26,27] framework. A plane-wave basis set with an energy cutoff of 420 eV and 13 × 13 × 13 k-point grid were used for the electronic self-consistent calculations. The structures were fully optimized until the maximum energy and force converged to less than 10^{-6} eV/Å and 1 meV/Å, respectively.

The phonon frequencies and electron–phonon coupling (EPC) were calculated using the Quantum-ESPRESSO (QE) package[28] within the framework of density functional perturbation theory (DFPT). Optimized norm-conserving Vanderbilt (ONCV) pseudopotentials[29] were employed, with a kinetic energy cutoff of 60 Ry and a charge density cutoff of 480 Ry. Self-consistent electron density and EPC calculations were performed using 24 × 24 × 24 k-point meshes and 6 × 6 × 6 q-point meshes. The T_c, the phonon spectrum, electronic bands, and density of states (DOS) of YB_2 with varying electron and hole concentrations were also computed using a 3 × 3 × 3 q-point grid, while retaining the same k-point grid as used for pure YB_2. Additionally, the isotropic Migdal–Eliashberg equations[18,19] were solved using the ELK code[30] in our study.

The T_c of YB_2, with effective Coulomb pseudopotential parameters (μ^*) ranging from 0.05 to 0.13 and under different concentrations of electron and hole doping, was calculated using the isotropic Migdal–Eliashberg equations, which are as follows:

$$Z(i\omega_n) = 1 + \frac{\pi T}{\omega_n}\sum_{n'}\frac{\omega_{n'}}{\sqrt{\omega_n^2 + \Delta^2(i\omega_n)}} \times \lambda(n-n'), \tag{1}$$

$$Z(i\omega_n)\Delta(i\omega_n) = \pi T\sum_{n'}\int\frac{\Delta(i\omega_{n'})}{\sqrt{\omega_n^2 + \Delta^2(i\omega_n)}} \times [\lambda(n-n') - \mu^*], \tag{2}$$

where $\omega_{n'}$ are the fermionic Matsubara frequencies and $\Delta(i\omega_n)$ is a superconducting gap, with renormalization function $Z(i\omega_n)$. Then, the Eliashberg spectral function is defined as

$$\alpha^2F(\omega) = \frac{1}{2\pi N(0)}\sum_{qj}\frac{\gamma_{qj}}{\omega_{qj}}\delta(\hbar\omega - \hbar\omega_{qj}), \tag{3}$$

where γ_{qj} stands for the phonon linewidth, and ω_{qj} represents the frequency with a phonon j with a wave-vector $\mathbf{q}$.

Allen and Dynes performed additional adjustments after McMillan's numerical analysis of the Eliashberg equation for numerous systems, yielding the following McMillan–Allen–Dynes formula:[20]

$$T_c = \frac{\omega_{\log}}{1.2}\exp\left[-\frac{1.04(1+\lambda)}{\lambda - \mu^*(1+0.62\lambda)}\right], \tag{4}$$

where μ^* is the effective Coulomb pseudopotential and can be set at a typical value of 0.1. The integrated electron–phonon coupling constant is

$$\lambda(\omega) = 2\int_0^{\omega}\frac{\alpha^2F(\omega)}{\omega}d\omega, \tag{5}$$

in which the electron–phonon coupling constant λ used in Eq. (1) is $\lambda(\omega_{\max})$, where $\omega_{\max}$ is the maximum of the phonon frequency. In addition, the logarithmically averaged characteristic phonon frequency $\omega_{\log}$ can be written as

$$\omega_{\log} = \exp\left[\frac{2}{\lambda}\int\frac{d\omega}{\omega}\alpha^2F(\omega)\ln(\omega)\right]. \tag{6}$$

In conclusion, the isotropic Migdal–Eliashberg equations are the source of the reduced McMillan–Allen–Dynes formula. By adding certain approximations, such as a simplified treatment of the phonon spectrum, it lowers the computing cost. Additionally, the two formulas have different areas of application. The isotropic Migdal–Eliashberg equations can precisely describe the microscopic

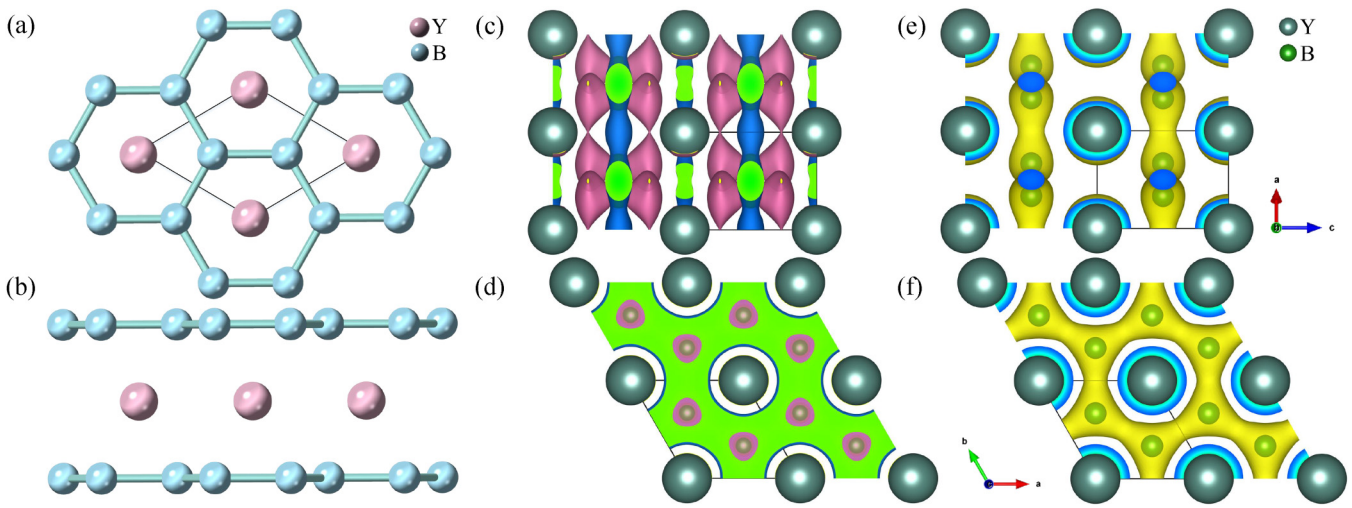

FIG. 1. The structural and electronic properties of YB_2: Top (a) and side (b) views of the atomic structure, with boron (B) represented by blue atoms and yttrium (Y) by pink atoms. For the side and top views, the charge density difference maps are displayed in (c) and (d), respectively, with purple denoting positive values and blue denoting negative values. Furthermore, (e) and (f) show the wave functions of YB_2, where boron (B) is represented by small atoms and yttrium (Y) by large atoms.

features of superconductors and is relevant to highly coupled superconductors. Nonetheless, the McMillan–Allen–Dynes equations are primarily utilized for a quick T_c estimate and works well for superconductors with modest coupling strengths.

III. RESULTS AND DISCUSSION

YB_2, with an AlB_2-type structure, belongs to the space group symmetry *P6/mmm* (No. 191). Its layered hexagonal crystal structure is illustrated in Figs. 1(a) and 1(b). The overall structure consists of two components: electron-gaining yttrium (Y) atoms and electron-losing boron (B) atoms. The crystal contains two types of sublattices: the upper layer has a hexagonal arrangement, while the other forms a rhombus structure. An intriguing finding is that boron atoms cluster together due to their strong bonding within the same boron layer and with the adjacent yttrium layers above and below. Preliminary analysis, shown in Figs. 1(c) and 1(d), highlights the strong interlayer interactions between boron atoms, which contribute to the superconductivity observed in YB_2, as indicated in Figs. 1(e) and 1(f).

The Fermi surface (FS) of YB_2 is composed of symmetrically closed ellipsoidal hole sheets at the A symmetry point, along with a uniformly open electron sheet, as depicted in Figs. 2(a)–2(c). From the FS diagram, the valley degeneracy (N_v) is determined to be 2, an exceptionally low value, indicating a low carrier concentration and effective mass in the density of states. The Brillouin zone, including the *k*-path, is shown in Fig. 2(d).

The corresponding electronic band structure of YB_2 is shown in Fig. 3(a). As evident from the figure, the orbitals near the Fermi level (E_F) are primarily composed of Y-*d* and B-*p* orbitals, with minimal contribution from Y-*p* orbitals. The lower T_c in YB_2 can be attributed to two factors. First, the Van Hove singularity is located 0.79 eV below the Fermi energy, which could contribute to the reduced T_c. These factors contribute to a low total density of states (DOS) at E_F, around 1.75 states/eV, which helps to explain the low T_c in the following.

The DOS of YB_2 at 0 GPa is shown in Fig. 3(b). The DOS is centered in the range of −4–1 eV. Additionally, the Y-*d* orbitals overlap with the B-*p* states and may even overlap with the B-*s* states, indicating a strong electronic interaction between Y and B

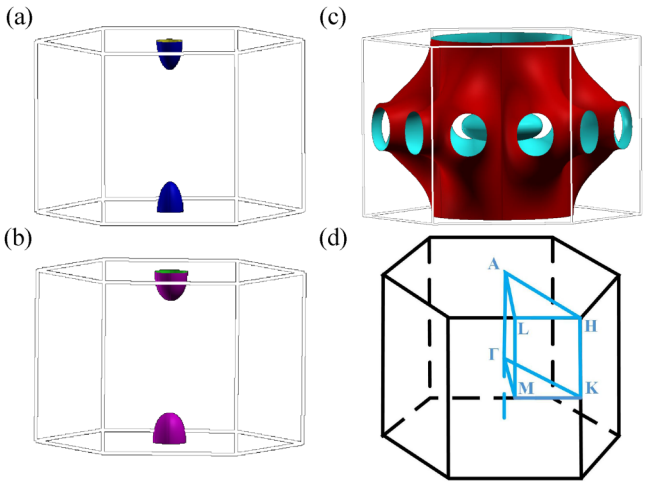

FIG. 2. The calculated Fermi surface of YB_2 around the A symmetry point is shown for the first energy band (a), the second energy band (b), and the third energy band (c). (d) The first Brillouin zone of YB_2, with the *k*-path marked by blue lines, consisting of high-symmetry points Γ, K, M, A, H, and L.

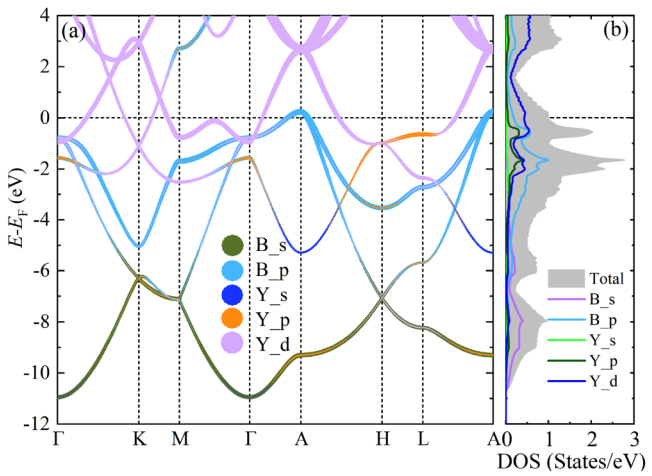

FIG. 3. The energy band structure and DOS of YB_2 are depicted in (a) and (b). In (a), the energy band diagram of YB_2 shows the contribution of different orbitals, where green, light-blue, dark-blue, orange, and purple dots represent the proportion of B-*s*, B-*p*, Y-*s*, Y-*p*, and Y-*d* orbitals, respectively. In (b), the total DOS of YB_2 is shown in shades of gray, with contributions from B-*s* orbitals in purple, B-*p* orbitals in light blue, Y-*s* orbitals in light green, Y-*p* orbitals in dark green, and Y-*d* orbitals in dark blue.

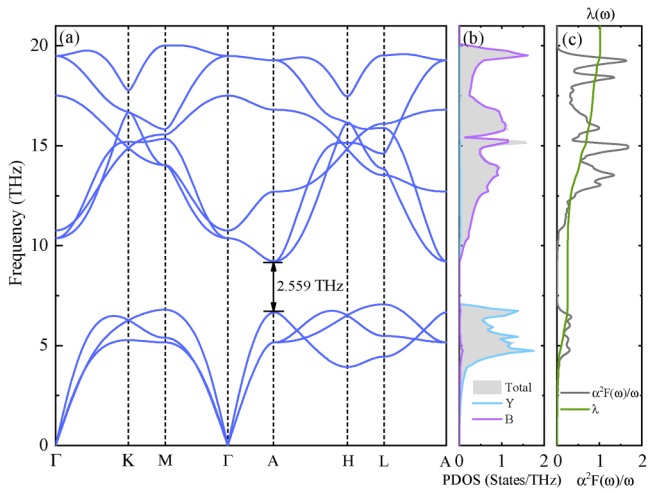

FIG. 4. The phonon spectrum, the projected phonon density of states (PDOS), the Eliashberg spectral function $\alpha^2F(\omega)$, and the electron–phonon coupling $\lambda(\omega)$ of YB_2 at ambient pressure are shown. (a) The phonon dispersion diagram is represented by dark-blue lines. (b) The total PDOS of YB_2 is shaded in light gray, with contributions from Y shown in light-blue lines and B in purple lines. (c) The Eliashberg spectral function α^2F (ω) is depicted in a dark gray line, alongside the electron–phonon coupling integral $\lambda(\omega)$ in green, for YB_2 at ambient pressure.

atoms. The central region of Fig. S1 in the supplementary material highlights the DOS at the Fermi energy level, which consists of B-*px*, *y*, *z* and Y-*dxy*,x^2,*yz* orbitals. The amplitude of these components is directly related to the strength of the electron–phonon coupling (EPC).

Figure 4(a) shows the phonon band structure of YB_2 at 0 GPa, demonstrating the dynamical stability of the structure. At the Γ symmetry point, the slopes of the longitudinal acoustic (LA) and transverse acoustic (TA) modes are 79.88 and 51.90, respectively, corresponding to phonon group velocities of 7.988 for LA and 5.19 km/s for TA. Additionally, a gap of 2.559 THz is observed between the acoustic and optical branches. Consistent with findings for ScB_2,[9] these calculations, along with the data in Fig. 2, suggest a small concentration of holes in YB_2, which could significantly influence the phonon properties and superconductivity of YB_2.

Further examination of the phonon density of states (PDOS) reveals that yttrium (Y) dominates the acoustic branch of the phonon dispersion, while boron (B) is predominant in the optical branch, as shown in Fig. 4(b), similar to the behavior observed in MgB_4.[31] Figure 4(c) indicates that high-frequency vibrations in the 12.5–20 THz range are the primary contributors to the EPC in YB_2, with the B element being the main source of these vibrations.

As shown in Fig. 5(a), the McMillan–Allen–Dynes formula and isotropic Eliashberg equations were used to calculate T_c. While the results from both methods are comparable, slight variations can be observed. In addition, experience-based μ^* ranges from 0.05 to 0.13. Figure 5(a) clearly shows a significant decline in T_c from the QE package as μ^* increases, particularly in the 0.05–0.1 range. This indicates that the computed T_c is significantly influenced by the numerical value of μ^*. Therefore, within the computational range, μ^* was selected to be closest to 0.1, which is the mean value of T_c. The different isotropic superconducting gaps Δ_0 of YB_2 on the Fermi surface, predicted using isotropic Migdal–Eliashberg equations and depicted as a function of temperature, are shown by the colored lines in Fig. 5(b). It is evident that the calculated T_c decreases as μ^* increases. Based on these observations, $\mu^* = 0.1$ was chosen, leading to a T_c for YB_2 of approximately 2.14 K.

As shown in Figs. 2 and 4, the analysis revealed that the hole concentration in YB_2 is low. To further investigate its superconducting properties, various electron and hole concentrations were computationally inserted, and the resulting T_c values are presented in Fig. 5(c). On the one hand, with the inclusion of holes, the T_c of YB_2 grows monotonically and quickly from 0 to 0.7 to a peak of 22.83 K. However, when holes are added, the T_c rapidly drops, with concentrations ranging from 0.7 to 0.8.

On the other hand, the number of electrons added decreases steadily from 0 to 0.3, as indicated by the negative concentrations in Fig. 5(c). Among the various methods of adding electrons or holes at different concentrations, it is evident that adding holes at a concentration of 0.7 has the most significant effect on increasing the T_c of YB_2, making it 7.15 times greater than the T_c without any additions. The steep rise in T_c with the addition of holes further supports the analysis that the hole concentration in Fig. 2 is insufficient, leading to the lower T_c observed for YB_2 in Fig. 5.

Moreover, the electron–phonon coupling strength (λ) and the logarithmically averaged characteristic phonon frequency (ω_{log}), both of which are proportional to T_c, are the primary parameters influencing the size of T_c according to Eq. (1). The trend of the

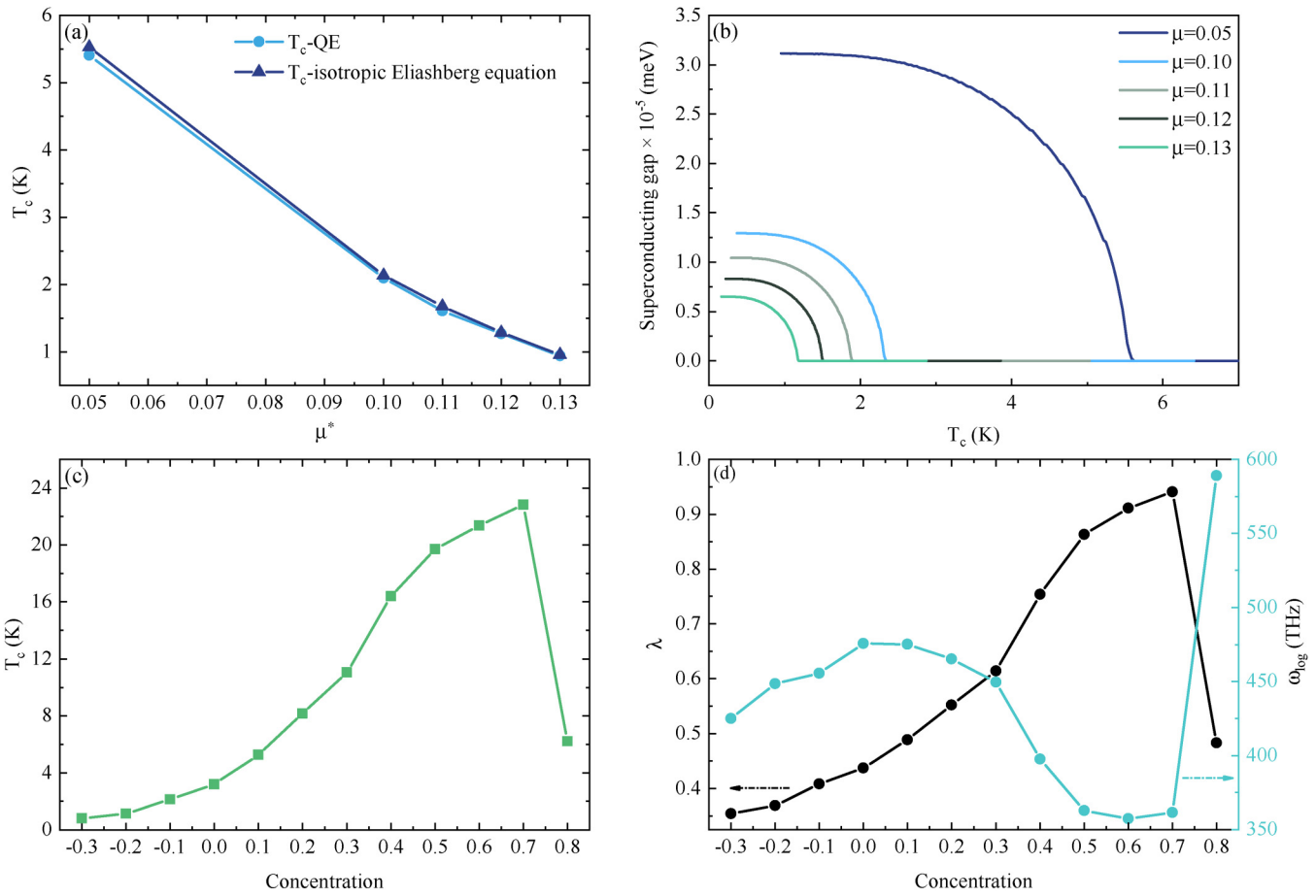

FIG. 5. The superconducting properties of YB_2. (a) The light-blue line stands for the result of T_c in the range of 0.05–0.13 by using QE package, while the dark-blue line represents the T_c using the isotropic Migdal–Eliashberg equation. (b) The isotropic superconducting gap of YB_2 at ambient pressure with different μ^*, where μ^* is equal to 0.05, 0.10, 0.11, 0.12, and 0.13 represented by light-green, dark-green, grayish green, light-blue, and dark-blue lines, respectively. (c) The green line stands for the result of T_c in different concentrations of added hole or electron by using the QE package, where a positive value means adding holes, while a negative one means adding electrons. (d) The trends of λ and ω_{log} of YB_2 following the addition of various electron or hole concentrations are shown by the aqua blue and black lines, respectively.

electron–phonon coupling strength in Fig. 5(d) for YB_2 with varying electron or hole concentrations is similar to that observed in Fig. 5(c). However, ω_{log} is smaller than that for pure YB_2 after adding either electrons or holes in 0.1–0.7, indicating that λ is a key determinant of T_c.

Figs. 6 and 7 show a comparison of the phonon spectra and energy bands with varying electron and hole concentrations. The phonons gradually become harder as the concentrations of hole rises, whereas the addition of electrons completely reverses the situation. Furthermore, with increasing hole concentrations, the region occupied by the peaks of the Eliashberg spectral function at the high-frequency optical phonon and the low-frequency acoustic phonon grows, until both diminish at 0.8 of increased hole concentrations. Additionally, it can be demonstrated that the T_c of YB_2 grows with increasing hole concentration up to 0.8 because the magnitude of the spectral function is related to the intensity of the electron–phonon coupling. Figures S2 and S3 in the supplementary material display these findings. Moreover, the results of the addition of electrons are precisely the reverse of those obtained by the addition of holes.

Surprisingly, the energy bands shown in Figs. 7(a) and 7(c) exhibit a similar overall trend. The general downward shift in the energy bands with increasing electron concentrations is reversed with the addition of holes. It can be observed that when the concentration of additional electrons grows, the Fermi energy level also increases, whereas the concentrations of hole drops. Figures 7(b) and 7(d) illustrate these results, where the total density of states (DOS) at the Fermi energy level decreases gradually with increasing electron concentration, but increases sharply with higher hole concentrations. These findings not only confirm the observations from Fig. 5(c) but also highlight that T_c for YB_2 can be further enhanced by increasing the hole concentrations.

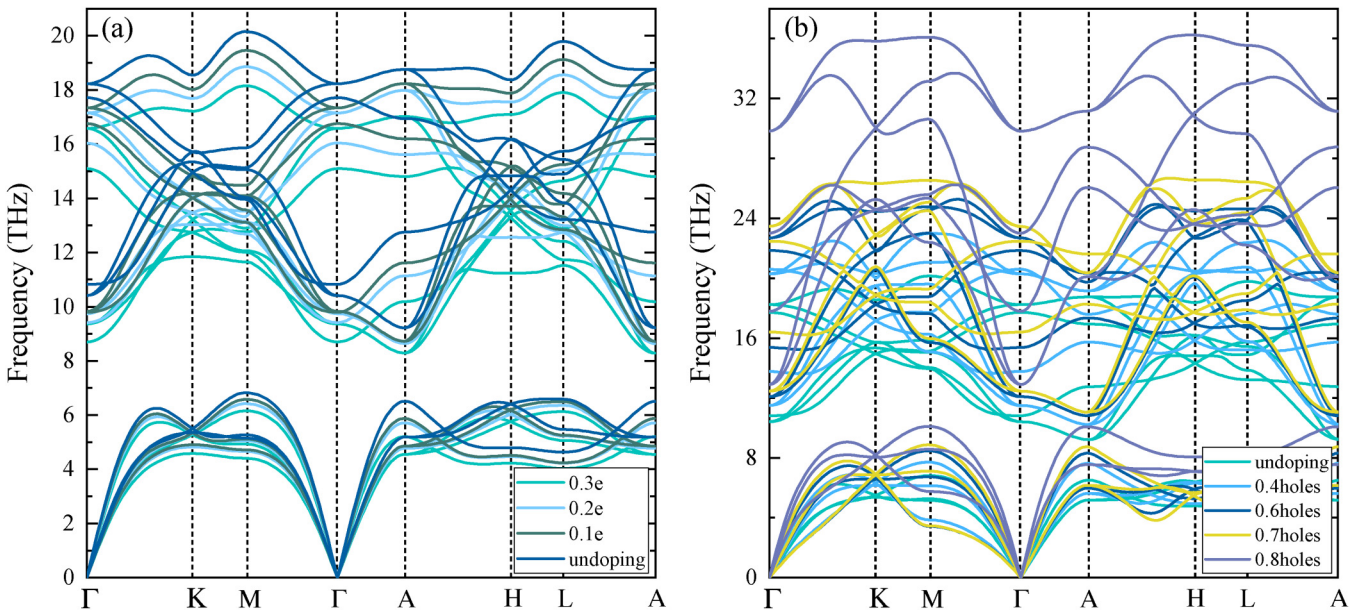

FIG. 6. The phonon spectrum of YB_2 is illustrated under different conditions. (a) The phonon spectrum with varying electron concentrations is shown: light-green lines represent the addition of 0.3 electrons, light-blue lines indicate the addition of 0.2 electrons, dark-green lines correspond to the addition of 0.1 electrons, and dark-blue lines represent the spectrum without any added electrons for comparison. (b) The phonon spectrum with varying concentrations of holes is depicted: light-blue, dark-blue, yellow, and purple lines represent the addition of 0.4, 0.6, 0.7, and 0.8 holes, respectively, while light-green lines correspond to the spectrum without any added holes.

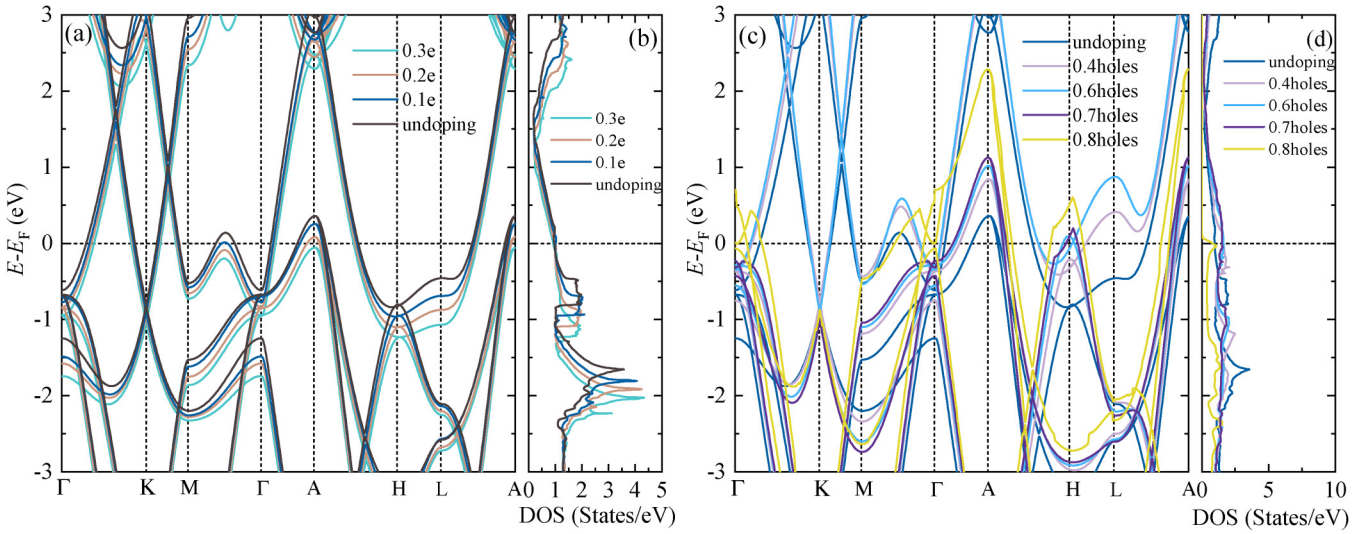

FIG. 7. The energy bands of YB_2 under different concentrations of added electrons and holes are illustrated. (a) The energy band structure with varying electron concentrations: light-blue lines represent the addition of 0.3 electrons, pink lines correspond to 0.2 electrons, dark-blue lines show the result of adding 0.1 electrons, and dark gray lines serve as a reference without added electrons. (b) The total density of states (DOS) for YB_2 under different electron concentrations, with the colored lines corresponding to the same electron concentrations as in (a). (c) The energy band structure with varying concentrations of added holes: light purple, light-blue, dark purple, and yellow lines represent the addition of 0.4, 0.6, 0.7, and 0.8 holes, respectively, while dark-blue lines represent the band structure without added holes. (d) The total DOS of YB_2 for varying hole concentrations, where the colored lines correspond to the same conditions as in (c).

TABLE I. The lattice constant and the corresponding T_c after adding different concentrations of electrons or holes is shown. Negative numbers indicate the addition of electrons, while positive numbers indicate the addition of holes.

Concentration	a or b (Bohr)	c (Bohr)	T_c (K)
−0.3	6.43	7.59	0.82
−0.2	6.36	7.48	1.15
−0.1	6.29	7.46	2.14
0	6.22	7.29	3.19
0.1	6.15	7.21	5.26
0.2	6.07	7.14	8.16
0.3	5.99	7.06	11.03
0.4	5.90	6.99	16.41
0.5	5.80	6.92	19.70
0.6	5.71	6.85	21.37
0.7	5.62	6.77	22.83
0.8	5.53	6.71	6.22

Another important finding is that this trend is supported by changes in lattice constants shown in Table I. The enhancement of electron–phonon coupling (EPC) induced by pressurization could be related to this result. Last, as illustrated in Fig. 8, the T_c of pure YB_2 and YB_2 with 0.7 holes added is compared with that of other boron-based compounds. Although the T_c of YB_2 is lower than that of MgB_2, it is higher than that of all other boron-based superconductors except $MoB_{2.5}$.[10] Additionally, with the incorporation of 0.7 holes, the T_c of YB_2 surpasses that of $MoB_{2.5}$. This comparison not only demonstrates that pure YB_2 has a higher T_c than many boron-related compounds but also highlights that T_c becomes significantly more remarkable when a sufficiently large number of holes are added.

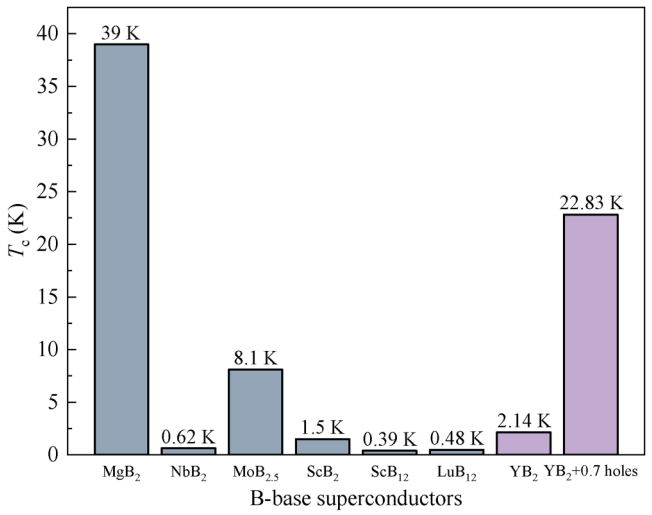

FIG. 8. The T_c of boron-related compounds at 0 GPa is illustrated, with gray bars representing data from the cited literature: MgB_2,[7] NbB_2,[8] $MoB_{2.5}$,[10] ScB_2,[9] ScB_{12}, and LuB_{12}.[32] The purple bars represent our calculated results.

IV. CONCLUSIONS AND DISCUSSIONS

In summary, we determine the precise range of the critical temperature (T_c) for a YB_2 crystal and investigate how electron and hole concentrations influence superconducting properties. We also find that varying concentrations of additional hole and electron can affect T_c. Based on the characteristics of bulk YB_2, we draw the following conclusions:

(i) When the parameter μ^* is 0.1, the T_c for YB_2 is identified as 2.14 K. Furthermore, T_c is expected to increase as μ^* decreases.
(ii) Similar to ScB_2, the superconducting properties of YB_2 are likely due to the close association of atoms in the B layer. The relatively low T_c is primarily attributed to a low concentration of holes rather than a lack of electrons.
(iii) The calculated T_c increases steadily with hole concentrations in the range of 0–0.8, reaching 22.83 K at 0.7. In contrast, the T_c decreases with added electron concentrations. This offers suggestions for enhancing the T_c of B-based materials that resemble MgB_2. Additionally, The T_c value shows an inverse correlation with the lattice constant of the crystal.

SUPPLEMENTARY MATERIAL

See the supplementary material for the sum of projected DOS for selected atoms and orbitals in YB_2, as well as the Eliashberg spectral function of YB_2 under varying electron or hole doping concentrations.

ACKNOWLEDGMENTS

We acknowledge the support from the National Natural Science Foundation of China (Nos. 12104356 and 52250191). Z.G. acknowledges the support of the Fundamental Research Funds for the Central Universities. This work was supported by the Key Research and Development Program of the Ministry of Science and Technology under Grant No. 2023YFB4604100. We also acknowledge the support by HPC Platform, Xi'an Jiaotong University.

AUTHOR DECLARATIONS

Conflict of Interest

The authors have no conflicts to disclose.

Author Contributions

Xuejie Li: Conceptualization (equal); Formal analysis (equal); Investigation (equal); Methodology (equal); Validation (equal); Visualization (equal); Writing – original draft (equal). **Wenbo Zhao:** Investigation (supporting); Methodology (supporting); Supervision (supporting); Visualization (equal); Writing – review & editing (supporting). **Yuzhou Hao:** Investigation (supporting). **Xiaoying Wang:** Investigation (supporting). **Zhibin Gao:** Writing – review & editing (equal). **Xiangdong Ding:** Writing – review & editing (supporting).

DATA AVAILABILITY

The data that support the findings of this study are available from the corresponding author upon reasonable request.

REFERENCES

[1]S. H. Autler, E. S. Rosenblum, and K. H. Gooen, "High-field superconductivity in niobium," Phys. Rev. Lett. **9**, 489–493 (1962).
[2]K. J. Chang and M. L. Cohen, "Electron-phonon interactions and superconductivity in Si, Ge, and Sn," Phys. Rev. B **34**, 4552–4557 (1986).
[3]B. T. Matthias, T. H. Geballe, K. Andres, E. Corenzwit, G. W. Hull, and J. P. Maita, "Superconductivity and antiferromagnetism in boron-rich lattices," Science **159**, 530 (1968).
[4]A. P. Drozdov, P. P. Kong, V. S. Minkov, S. P. Besedin, M. A. Kuzovnikov, S. Mozaffari, L. Balicas, F. F. Balakirev, D. E. Graf, V. B. Prakapenka, E. Greenberg, D. A. Knyazev, M. Tkacz, and M. I. Eremets, "Superconductivity at 250 K in lanthanum hydride under high pressures," Nature **569**, 528–531 (2019).
[5]S. Cross, J. Buhot, A. Brooks, W. Thomas, A. Kleppe, O. Lord, and S. Friedemann, "High-temperature superconductivity in La_4H_{23} below 100 GPa," Phys. Rev. B **109**, L020503 (2024).
[6]S. Chen, J. Guo, Y. Wang, X. Wu, W. Chen, X. Huang, and T. Cui, "Synthesis and superconductivity in (La, Ca)H_{10} under high pressure," Phys. Rev. B **109**, 224510 (2024).
[7]J. Nagamatsu, N. Nakagawa, T. Muranaka, Y. Zenitani, and J. Akimitsu, "Superconductivity at 39 K in magnesium diboride," Nature **410**, 63–64 (2001).
[8]L. Leyarovska and E. Leyarovski, "A search for superconductivity below 1 K in transition metal borides," J. Less-Common Met. **67**, 249–255 (1979).
[9]S. M. Sichkar and V. N. Antonov, "Electronic structure, phonon spectra and electron–phonon interaction in ScB_2," Low Temp. Phys. **39**, 595–601 (2013).
[10]A. S. Cooper, E. Corenzwit, L. D. Longinotti, B. T. Matthias, and W. H. Zachariasen, "Superconductivity: The transition temperature peak below four electrons per atom," Proc. Natl. Acad. Sci. U.S.A. **67**, 313–319 (1970).
[11]X. Liu, X. Huang, P. Song, C. Wang, L. Zhang, P. Lv, L. Liu, W. Zhang, J.-H. Cho, and Y. Jia, "Strong electron-phonon coupling superconductivity in compressed $\alpha - MoB_2$ induced by double Van Hove singularities," Phys. Rev. B **106**, 064507 (2022).
[12]H. J. Choi, S. G. Louie, and M. L. Cohen, "Prediction of superconducting properties of CaB_2 using anisotropic Eliashberg theory," Phys. Rev. B **80**, 064503 (2009).
[13]N. I. Medvedeva, A. L. Ivanovskii, J. E. Medvedeva, and A. J. Freeman, "Electronic structure of superconducting MgB_2 and related binary and ternary borides," Phys. Rev. B **64**, 020502 (2001).
[14]X. L. Chen, Q. Y. Tu, M. He, L. Dai, and L. Wu, "The bond ionicity of MB_2 (M = Mg, Ti, V, Cr, Mn, Zr, Hf, Ta, Al and Y)," J. Phys.: Condens. Matter **13**, L723 (2001).
[15]C. Li, F. Xu, B. Li, J. Li, G. Li, K. Watanabe, T. Taniguchi, B. Tong, J. Shen, L. Lu, J. Jia, F. Wu, X. Liu, and T. Li, "Tunable superconductivity in electron-and hole-doped bernal bilayer graphene," Nature **631**, 300–306 (2024).
[16]A. N. Rudenko, D. I. Badrtdinov, I. A. Abrikosov, and M. I. Katsnelson, "Strong electron-phonon coupling and phonon-induced superconductivity in tetragonal C_3N_4 with hole doping," Phys. Rev. B **109**, 014502 (2024).
[17]J. Choi, S. Tu, A. Nag, C. C. Tam, S. Tippireddy, S. Agrestini, Z. Lin, M. Garcia-Fernandez, K. Jin, and K.-J. Zhou, "Unified description of charge density waves in electron-and hole-doped cuprate superconductors," arXiv:2407.15750 (2024).
[18]J. A. Flores-Livas, L. Boeri, A. Sanna, G. Profeta, R. Arita, and M. Eremets, "A perspective on conventional high-temperature superconductors at high pressure: Methods and materials," Phys. Rep. **856**, 1–78 (2020).
[19]K. P. Hilleke and E. Zurek, "Tuning chemical precompression: Theoretical design and crystal chemistry of novel hydrides in the quest for warm and light superconductivity at ambient pressures," J. Appl. Phys. **131**, 070901 (2022).
[20]P. B. Allen and R. C. Dynes, "Transition temperature of strong-coupled superconductors reanalyzed," Phys. Rev. B **12**, 905–922 (1975).
[21]G. Kresse and J. Furthmüller, "Efficiency of ab-initio total energy calculations for metals and semiconductors using a plane-wave basis set," Comput. Mater. Sci. **6**, 15–50 (1996).
[22]G. Kresse and J. Furthmüller, "Efficient iterative schemes for *ab initio* total-energy calculations using a plane-wave basis set," Phys. Rev. B **54**, 11169–11186 (1996).
[23]J. P. Perdew, K. Burke, and M. Ernzerhof, "Generalized gradient approximation made simple," Phys. Rev. Lett. **77**, 3865–3868 (1996).
[24]J. A. White and D. M. Bird, "Implementation of gradient-corrected exchange-correlation potentials in Car-Parrinello total-energy calculations," Phys. Rev. B **50**, 4954–4957 (1994).
[25]Z. Wu and R. E. Cohen, "More accurate generalized gradient approximation for solids," Phys. Rev. B **73**, 235116 (2006).
[26]G. Kresse and J. Hafner, "*Ab initio* molecular dynamics for open-shell transition metals," Phys. Rev. B **48**, 13115–13118 (1993).
[27]P. E. Blöchl, "Projector augmented-wave method," Phys. Rev. B **50**, 17953–17979 (1994).
[28]P. Giannozzi, S. Baroni, N. Bonini, M. Calandra, R. Car, C. Cavazzoni, D. Ceresoli, G. L. Chiarotti, M. Cococcioni, I. Dabo, A. D. Corso, S. de Gironcoli, S. Fabris, G. Fratesi, R. Gebauer, U. Gerstmann, C. Gougoussis, A. Kokalj, M. Lazzeri, L. Martin-Samos, N. Marzari, F. Mauri, R. Mazzarello, S. Paolini, A. Pasquarello, L. Paulatto, C. Sbraccia, S. Scandolo, G. Sclauzero, A. P. Seitsonen, A. Smogunov, P. Umari, and R. M. Wentzcovitch, "QUANTUM ESPRESSO: A modular and open-source software project for quantum simulations of materials," J. Phys.: Condens. Matter **21**, 395502 (2009).
[29]M. Schlipf and F. Gygi, "Optimization algorithm for the generation of ONCV pseudopotentials," Comput. Phys. Commun. **196**, 36–44 (2015).
[30]See http://elk.sourceforge.net/ for "The Elk Code."
[31]J. Bekaert, M. Petrov, A. Aperis, P. M. Oppeneer, and M. V. Milošević, "Hydrogen-induced high-temperature superconductivity in two-dimensional materials: The example of hydrogenated monolayer MgB_2," Phys. Rev. Lett. **123**, 077001 (2019).
[32]B. T. Matthias, T. H. Geballe, K. Andres, E. Corenzwit, G. W. Hull, and J. P. Maita, "Superconductivity and antiferromagnetism in boron-rich lattices," Science **159**, 530 (1968).